Comparative Proteomic Analysis of Advanced Ovarian Cancer Tissue to Identify Potential Biomarkers of Responders and Nonresponders to First-Line Chemotherapy of Carboplatin and Paclitaxel

Urmila Sehrawat[1,*], Ruchika Pokhriyal[1,*], Ashish Kumar Gupta[1], Roopa Hariprasad[2], Mohd Imran Khan[1], Divya Gupta[1], Jasmine Naru[3], Sundararajan Baskar Singh[1], Ashok Kumar Mohanty[3], Perumal Vanamail[4], Lalit Kumar[2], Sunesh Kumar[4] and Gururao Hariprasad[1]

[1]Department of Biophysics, All India Institute of Medical Sciences, Ansari Nagar, New Delhi, India. [2]Department of Medical Oncology, All India Institute of Medical Sciences, Ansari Nagar, New Delhi, India. [3]National Dairy Research Institute, Karnal, India. [4]Department of Obstetrics and Gynecology, All India Institute of Medical Sciences, Ansari Nagar, New Delhi, India. *These authors have contributed equally to this work.

ABSTRACT: Conventional treatment for advanced ovarian cancer is an initial debulking surgery followed by chemotherapy combination of carboplatin and paclitaxel. Despite initial high response, three-fourths of these women experience disease recurrence with a dismal prognosis. Patients with advanced-stage ovarian cancer who underwent cytoreductive surgery were enrolled and tissue samples were collected. Post surgery, these patients were started on chemotherapy and followed up till the end of the cycle. Fluorescence-based differential in-gel expression coupled with mass spectrometric analysis was used for discovery phase of experiments, and real-time polymerase chain reaction, Western blotting, and pathway analysis were performed for expression and functional validation of differentially expressed proteins. While aldehyde reductase, hnRNP, cyclophilin A, heat shock protein-27, and actin are upregulated in responders, prohibitin, enoyl-coA hydratase, peroxiredoxin, and fibrin-β are upregulated in the nonresponders. The expressions of some of these proteins correlated with increased apoptotic activity in responders and decreased apoptotic activity in nonresponders. Therefore, the proteins qualify as potential biomarkers to predict chemotherapy response.

KEYWORDS: advanced ovarian cancer, gel-based proteomics, biomarkers, chemotherapy response, apoptotic pathways

Introduction

Ovarian cancer is an important cause of morbidity and mortality. During the year 2012, it ranked fourth in frequency among all cancers in women, with an estimated 26,834 new cases occurring in India and was responsible for 19,549 deaths in the same year.[1,2] The ovarian cancers are staged using Federation of International Gynecology and Obstetrics (FIGO) system that is based on the extent of tissue involvement, lymph node status, and magnitude of metastasis. Accordingly, stage I and stage II cancers confined to the pelvic cavity are termed as early-stage ovarian cancer. The stage III and stage IV cancers are those that have spread beyond the pelvic cavity and are termed advanced ovarian cancer. Approximately, three-fourths of epithelial ovarian cancers are detected at an advanced stage.[3]

Patients with advanced ovarian cancer are conventionally treated by primary cytoreductive debulking surgery followed by adjuvant chemotherapy that includes a platinum agent of either carboplatin or cisplatin combined with a taxane agent

of paclitaxel or docetaxel.[4] Platinum-based drugs are inorganic in nature and form square planar complexes with DNA, which are known as platin-DNA adducts that cause physical distortions that culminate in irreversible apoptotic pathway.[5] Paclitaxel targets microtubules, wherein they bind to the microtubule polymer, enhancing the polymerization of tubulin and altering the kinetics of microtubules.[6,7] This chemotherapeutic combination regimen produces complete clinical response in the range of 60%–80%.[8] However, subsequently, recurrences occur in the majority of cases, resulting in dismal prognosis with low survival rates of 30%–50% at five years.[9] Retrospective studies of these chemotherapy combination-based therapies have identified two subgroups of patients with recurrent ovarian cancer. Those who relapse within six months are considered resistant and those who are disease free for at least six months are considered sensitive to following a response to first-line chemotherapy.[10,11]

Relapse that is seen in the patients are mostly due to drug resistance. Resistance to chemotherapy is environmental,

acquired, or intrinsic in nature. Environment resistance or de novo resistance is one in which tumor cells are transiently protected from chemotherapy-induced apoptosis via the induction of survival signaling pathways such as the role of soluble factors in the tumor microenvironment.[12] Acquired resistance is due to successive chemotherapy exposures, where cells that were initially sensitive to a drug adapt for survival after prolonged exposure to the drug.[13] In contrast, intrinsic resistance is observed when the tumor cells are resistant to a drug without any prior exposure.

Various approaches such as functional genomics, systems biology, and proteomics have been used so far in order to look into the differential ways by which ovarian cancerous cells are continuously developing resistance toward chemotherapeutic drugs. Most of the studies done so far have been on cancer cell lines, which addressed acquired resistance to chemotherapy.[14,15] These studies pose a chance of mutation-induced protein expression for erroneous functional attributes due to which clinical relevance is lost. Clinical proteomics that involves protein profiling of tissue samples from patients is an effective approach and holds promise to delineate protein signatures in advanced ovarian cancer.[16] Two-dimensional-differential in-gel expression (2D-DIGE) is a form of protein profiling where three different protein samples can be labeled with size-matched, charge-matched spectrally resolvable fluorescent cyanine (Cy) dyes prior to 2D electrophoresis.[17] This technique provides the advantage of comparing protein profiles of tissues from different clinical profiles on the same gel, thereby overcoming the limitation due to inter-gel variation.[18] Therefore, this experiment holds scope to compare innate tissue protein signatures in chemotherapy-resistant and -sensitive advanced ovarian cancer patients.

The many advantages of differentiating these two conditions are as follows: (1) an early indication to chemotherapy response will help to plan an effective regimen right after the cytoreductive surgery; (2) a range of alternative chemotherapy with newer drugs, stem cells, and immunotherapy can be incorporated to improve the survival duration of those who are resistant.,[19–21] and (3) from the patient's perspective, it will help to efficiently use financial expenditure and time, that is so very crucial in the treatment of advanced ovarian cancer. The differential display and relative quantification of protein biomarkers in this study will not only help to understand the biology of drug response but will also lay a translational platform for the design of diagnostic pharmacotherapy of ovarian cancer.

Methods

Ethics, consent, and sample collection. The study was approved by the ethics committee of All India Institute of Medical Sciences (Reference: IEC/NP-23/2013), and the procedures followed were in accordance with the ethical standards formulated in the Declaration of Helsinki. The patients were screened and admitted at the Department of Obstetrics and Gynecology. Patients with advanced-stage ovarian cancer who underwent primary debulking surgery were recruited. Written informed consents were taken from these patients before enrolling them into the study. Patient names and file numbers were kept confidential, and unique identification codes were given. As per the departmental protocol, a detailed workup of patients suspected of having advanced-stage primary epithelial ovarian cancer included computer-assisted tomography (CAT) scan of the abdomen and pelvis, CA125 monitoring, and ascitic fluid cytology. Upper gastroendoscopy and lower gastroendoscopy were done to rule out primary gastro-intestinal metastasis to ovary. Tissue samples were collected as blocks of 2 g. Adherent connective tissues were neatly dissected, and blood stains were removed by washing thoroughly with 1× phosphate-buffered saline (PBS) and tissues were stored at −70°C. Samples were simultaneously also sent to Department of Pathology for histopathological confirmation of tumor. Postoperative CAT scans of the abdomen and pelvis were repeated to document the residual disease. Subsequent to postoperative recovery, patients were registered at the Department of Medical Oncology and started on chemotherapy regimen comprising six cycles of carboplatin and paclitaxel. Paclitaxel was administered intravenously over three hours at a dose of 175 mg/m^2 followed by carboplatin at a dose of 75 mg/m^2. The treatment regimen was followed every four weeks for six cycles. The patients were followed up with routine investigations of computer tomography and CA125 monitoring till the end of the cycle to assess their chemotherapy response. Following completion of primary treatment, the stored tissue samples were retrospectively labeled as either responders or nonresponders based on patient inclusion and exclusion criteria.

Patient inclusion and exclusion criteria. Chemotherapy outcomes were based on the revised RECIST guidelines (version 1.1) for response evaluation criteria in solid tumors. Responders were those with complete response having disappearance of all known diseases on clinical and radiological examination. Nonresponders were those with partial response, progressive disease, or stable disease. Partial responders were those having at least 30% reduction in the sum of target lesions taking as reference the baseline sum diameters. Patients with progressive disease were those having 20% increase in the sum of diameters of target lesions, taking as reference the smallest sum on study or the appearance of one or more new lesions, including the appearance of pleural effusion or ascitic fluid. Stable responders were those patients who were between the above two categories. In addition, the Gynecologic Cancer Intergroup-CA125 progression criteria were integrated to tumor response assessment criteria. At the end of the sixth cycle, normalization of CA-125 (<35 μ/mL) was considered as responders, and persistent high levels with ≥35 μ/mL were considered as nonresponders. Chemotherapy was discontinued to patients diagnosed to be having progressive disease and they were put on second-line chemotherapy.

The exclusion criteria were those patients who received neo-adjuvant chemotherapy before surgery to reduce tumor load.

Patient recruitment. Treatment of advanced-stage ovarian cancer involves a debulking surgery followed by six cycles of chemotherapy combination comprising platinum agent and taxol agent. Thirty-two patients with stage IIIC or stage IV advanced ovarian cancer (FIGO ovarian cancer staging) were recruited in the study and underwent debulking surgery at the Department of Obstetrics and Gynecology. Subsequent to their postoperation recovery, the patients were recruited at the Department of Medical Oncology for chemotherapy. During the period of chemotherapy, eight of them were found ineligible, five were lost to follow-up, and three died during treatment. In the postchemotherapy follow-up, three patients had clinically and radiologically proven disease-free state along with normalization of CA125 (<35 units). The tissue samples procured from these patients were labeled as responders. Two patients developed new lesions, one had radiological evidence of tumor lesion, and two had persistent high levels of CA125 at the end of chemotherapy regimen. Tissue samples that were procured from these five patients were labeled as nonresponders.

Sample processing and 2D electrophoresis standardization. The samples stored at –70°C were labeled as either responders or nonresponders after assessment of the patients at the end of chemotherapy cycle. The tissue samples were minced, and the proteins were solubilized in 100 µL of lysis buffer containing 8M urea, 2M thiourea, and 4% 3-[(3-Cholamidopropyl)dimethylammonio]-1-propanesulfonate (CHAPS). The samples were centrifuged at 4,000 rotations per minute (rpm) for five minutes, and the supernatant was taken for experiments. The protein concentration of samples was estimated by Bradford method using bovine serum albumin (BSA) as standard. 2D elecrophoretic experiments were standardized for the collected set of ovarian cancer tissue samples.[22,23]

2D-DIGE. A total of 50 µg of protein from each pool of responders and nonresponders were labeled with Cy dye flours according to minimal labeling protocol provided by the manufacturer (Amersham Biosciences). Two sets of responder samples were labeled with 200 pmol of Cy3, and two sets of nonresponder samples were labeled with 200 pmol of Cy5. For the third set, dye swapping was done where the responder protein sample was labeled with 200 pmol of Cy5 and non-responder protein sample was labeled with 200 pmol of Cy3. Equal amount of protein from both subsets was mixed to generate an internal standard, and 50 µg of protein from this internal standard was labeled with 200 pmol of Cy2. Therefore, each of the proposed gels consisted of responder (Cy3 or Cy5), nonresponder (Cy5 or Cy3), and one internal standard (Cy2) sample. Labeled samples of responder, nonresponder, and internal standard were pooled together, and rehydrating stock solution (8M urea, 2M thiourea, 2% CHAPS and 0.002% bromophenol blue) was added to make up the final volume to 250 µL. Dithiothreitol (DTT) and immobilized

pH gradient (IPG) buffer (pH 3–10) were added to final concentrations of 0.003% and 0.5%, respectively. After mixing, samples were centrifuged at 4,000 rpm for two minutes to remove any particulate matter. The solution was then loaded on a reswelling tray (Amersham Biosciences). *Immobiline Dry Gel Strip* of pH range 3–10, 13 cm was used for isoelectric focusing. Plastic cover on the strip was carefully removed, and the gel surface was placed over the sample in the tray with forceps. The gel strips were overlaid with Iso-Electric Focusing (IEF) cover fluid (Amersham Biosciences) and were kept overnight for 15 hours for optimum rehydration. Rehydrated IPG strips was kept in a strip holder and subjected for IEF in an *Ettan IPGphor 3* IEF system (Amersham Biosciences) as per the following program: (1) step mode, 150 V for 30 minutes; (2) step mode, 500 V for 30 minutes; (3) step mode, 1,000 V for 30 minutes; (4) gradient mode, 4,000 V for 2 hours; (5) step mode, 4,000 V for 2 hours; (6) gradient mode, 6,000 V for 2 hours; (7) step mode, 6,000 V till total volt-hours of 28,000 was achieved. Each electro focused strip was equilibrated, first with 10 mL of sodium deodyl sulfate (SDS) buffer containing 10 mg/mL DTT for 15 minutes. This was followed by second equilibration with 10 mL of SDS buffer containing 25 mg/mL iodoacetamide for 15 minutes. The strips were then transferred onto 10% homogenous polyacrylamide gels cast on *SE 600 Ruby* gel apparatus (GE Healthcare). The strips were overlaid with 0.5% agarose sealing solution (0.5% agarose, 0.002% bromophenol blue in Tris-glycine electrode buffer). Separation in sodium deodyl sulfate poly-acrylamide gel electrophoresis (SDS-PAGE) was carried out with constant running current set at 15 mA per gel at 20°C for 30 minutes, followed by 30 mA per gel at 20°C until the bromophenol blue dye front ran off from the bottom of the gels. Three such gels were run as replicates.

Gel imaging, spot detection, and statistical analysis. Labeled proteins were visualized using a *Typhoon TRIO Variable Mode Imager* (GE Healthcare). Cy2 images were scanned with 488 nm/520 nm band pass, Cy3 images were scanned with 532 nm/580 nm band pass, and Cy5 images were scanned with 633 nm/670 nm band pass. All gels were scanned with a photon multiplier tube (PMT) setting of 500–600 V with 100 µm/pixel resolution. Images were cropped using *ImageQuant v5.5 loader module of DeCyder 2D* software (GE Healthcare) to remove areas extraneous to the gel image. Three images were obtained from each gel corresponding to responder, nonresponder, and internal standard. These gel images were processed for spot detection and quantification in DIA mode of *DeCyder software 7.0* (GE Healthcare). The imported images created three different workspaces for each of the three gel pairs. The maximum number of spots for each codetection procedure was set to 1,500, and the gel with the highest count was assigned as the master gel. Artifacts of dust particles and protein streaks were manually removed from analysis. The intensity of spots in the Cy3 and Cy5 images were normalized to that of Cy2 image in

the same gel. The spots were codetected and quantified automatically as 2-D-DIGE image pairs, intrinsically linking the samples to its in-gel standard. These three DIA workspaces were then analyzed in the *biological variance analysis* (BVA) workspace. In BVA work space, each Cy3 or Cy5 gel image was assigned an experimental condition as either responder or nonresponder, and all Cy2 images were taken as standards. Using Cy3:Cy2 and Cy5:Cy2 DIA ratios, average abundance changes and Student's *t*-test *P*-values were calculated. Only those spots with 1.5 ratio differences in volume after normalization between Cy3 and Cy5 and a *P*-value <0.05 were defined as spots of interest. Matching between gels was performed utilizing the in-gel standard from each image pair and further improved by land marking and manually confirming potential spots of interest.

Mass spectrometric analysis and protein identification. A preparative gel was run using 300 μg of protein and stained with colloidal Coomassie Blue G250 stain. Matched spots of interest were picked manually from the preparative gel. These spots were subjected to in-gel trypsinization according to the manufacturer's protocol (Promega). After overnight digestion, digestion buffer containing the peptides was recovered. Additional extraction of peptides was carried out with 100 μL of 50% acetonitrile in 1% formic acid. The extracts were pooled and vacuum dried and stored in 4°C refrigerator. At the time of analysis, the peptide extract were reconstituted in 10 μL of 60% acetonitrile and 0.1% trifluoroacetic acid (TFA). The peptides were mixed with α-cyano-4-hydroxycinnamic acid matrix in a ratio of 1:1 and spotted on the matrix-assisted laser desorption ionization (MALDI) plate. MALDI-mass spectrometry (MS) data were acquired automatically over a mass range of 800–3,500 Da in the reflector ion mode on a *4800 MALDI*-time of flight *(TOF)/TOF Analyzer* (Applied Biosystems) with *4000 Series Explorer v3.5 software*, using a fixed laser intensity for 1,500 shots/spectrum, with a uniform random spot search pattern. The potential difference between acceleration voltage and floating collision cell defines the collision energy, which was 1 keV in all experiments. Reoptimized instrument settings were employed to achieve optimal sensitivity. Air was used as the collision gas such that nominally single collision conditions were achieved. In each MS spectrum, the 10 most abundant MS peaks were selected for MS/MS using an acquisition method that excluded ions with S/N less than 50, and which filtered out identical peaks detected in adjacent spots, selecting only the strongest precursor. The precursor ions with the weakest S/N were acquired first in order to achieve the maximum signal intensity for low-abundance peptides. A 1 kV MS/MS operating mode was used, the relative precursor mass window was set at 250 (full-width half mass), with metastable suppression enabled. MS/MS acquisition of selected precursors was set to a maximum of 1,250 shots with 50 shots per subspectrum using fixed laser intensity. The stop-condition criteria were set to a minimum of 100 S/N on more than seven peaks within

the spectrum after the minimum 1,000 shots. To identify the peptide, peptide masses obtained from the MS analysis were searched in MASCOT search engine with NCBI nr database for the identification of proteins. Detected protein threshold was fixed at confidence score of 99.9%.

Pathway analysis. All the information of genes corresponding to identified proteins and their related functions were searched from NCBI and UniProt. Based on this information, the proteins were studied for their biological interaction network in apoptosis and cancer pathways using KEGG database.[24] The Cytoscape v2.8.0 software[25,26] and plugin Michigan Molecular Interactions[27] were used to gather and merge human gene regulatory interactome from well-known databases, including BIND, MINT, and HPRD.[28–30] From this complete network, subnetworks for apoptosis and cancer were extracted up to the second neighboring nodes using the plugin BiNoM v2.5. The resulting networks were merged using Cytoscape. Venn/Euler diagram was used to delineate the intersection between apoptotic and cancer pathways, and the interactions of the identified proteins were noted.

RNA isolation and cDNA synthesis. A total of 50 mg of ovarian cancer tissues from three responders and three nonresponders to standard first-line chemotherapy were taken. Total cellular RNA was extracted from homogenized tissues using Trizol reagent (Amresco). The quality and quantity of RNA was estimated by taking an absorbance ratio of 260 nm:280 nm above 1.8 using Nanodrop spectrophotometer (benchtop). A total of 150 ng of total RNA from was taken from each sample for cDNA preparation using cDNA Synthesis Kit (Thermo Scientific) provided with anchored oligo-dT primer. Reverse transcription was performed on thermocycler (GenePro). Quality of cDNA was checked using glyceraldehyde 3-phosphate dehydrogenase (GAPDH) primers and stored at −20°C for further use.

Quantitative real-time PCR. Primers for heat shock protein (HSP)-27, α-enolase, caspase 3, caspase 8, cytochrome C, and GAPDH were designed based on the nucleotide sequences at NCBI. The primers were tested empirically for amplification from 100 ng of cDNA. The relative amplification efficiencies of the primers were tested and found to be similar. Quantitative real-time PCR reactions were performed using specific protocol (DyNaMo color flash master mix; Thermo Scientific) on CFX96 machine (Bio-Rad) as per manufacturer's instructions. For SYBR Green based PCR reaction (Bio-Rad), the reaction contained, 5 pmol forward and reverse primers, 100 ng cDNA SYBR Green mix, and water added upto 20 μL. The PCR cycling parameters were set up for 39 reaction cycles that included denaturation at 95°C for 7 minutes, annealing at 58°C for 20 seconds, and extension at 72°C for 15 seconds. After amplification, a melting curve analysis was performed by collecting fluorescence data. All the program parameters and acquisition of data were done by CFX manager software (version 1.6). Glyceraldehyde

3-phosphate dehydrogenase (GAPDH) was used as an internal reference housekeeping gene for the normalization of the expression and sample PA676 was used as reference internal standard. ΔΔ cycle threshold (CT) algorithm was used to analyze the relative mRNA expression. All tests were performed in duplicate. Data analysis was carried out using IBM SPSS Statistics-20 software. Descriptive measures such as mean, median, and standard deviations of each relative mRNA expression were calculated for responders and nonresponders. Mean and standard deviation were plotted in histogram with plus one standard deviation. Correlation analysis was done for mRNA expressions of HSP-27 and enolase, with caspase 3, caspase 8, and cytochrome C. Correlation coefficient (r) was calculated to ascertain the strength of relationship.

Western blot analysis. Western blotting was done on six ovarian cancer tissue samples. About 20 μg of protein samples was resolved by 12% SDS-PAGE and transferred to nitrocellulose membrane (MDI) by wet transfer method using Mini Protean I (Bio-Rad Laboratories) with a constant current of 0.2 A for one hour at 4°C. Membrane was blocked with 5% bovine serum albumin in 1× PBS for one hour at room temperature. It was then washed with PBST (0.05% Tween 20 in 1× PBS) thrice for 10 minutes each. Mouse primary antibodies for alpha enolase (Santa Cruz Biotechnology) at 1:1,000 dilution was used for incubation at 4°C for 12 hours. Membrane was washed thrice with PBST and incubated with anti-mouse antibody conjugated with horseradish peroxidase (Santa Cruz Biotechnology) diluted to 1:5,000. After incubation for one hour at room temperature, it was washed with PBST and developed with diaminobenzidine (25 mg/mL) dissolved in PBS containing H_2O_2 (0.3% w/v). A semiquantitative analysis based on optical density was performed by ImageJ software.

Results and Discussion

Clinical profile. The clinical data of eight patients in the study group are provided in Table 1. Six of them had papillary serous cyst adenocarcinoma, one had poorly differentiated endometroid adenocarcinoma, and one had clear cell carcinoma. It is interesting to note that one of the patients who revealed no radiological evidence of disease had a CA125 concentration of 112 units. The sustained high levels of CA125 have been known to have high correlation with subclinical ovarian cancer disease state. It may be noted that tissue samples were retrospectively labeled as either responder or nonresponder based on the defined criteria of chemotherapy outcomes. This implied to the fact that tissues were not exposed to the chemotherapy at the time of procurement, and therefore the identified protein signatures are indicative of innate body response mechanisms to carboplatin–paclitaxel combination.

2D-DIGE. Proteins were isolated from the tissues for comparative gel-based proteomic experiments. The initial standardization experiments included ovarian cancer tissue protein quantification and assessment of possible ionic and soluble lipid impurities in the sample. It was inferred that concentrations of salt and soluble lipid in ovarian cancer tissue did not affect the resolution of spots on 2D electrophoresis.[22,23] The proteins were labeled with Cy dyes for the DIGE experiment with experimental triplicates. Three images corresponding to three samples (responders, nonresponders, and internal standard) were generated for each gel. The images of three combined gels and their corresponding three label specific images are shown in Figure 1. A total of nine images generated show a very uniform and similar distribution of spots consistently present across the three gels. The number of spots ranged between 650 and 700 across the gels and was

Table 1. Clinical profile of patients with advanced ovarian cancer and their treatment response.

| PATIENT ID	AGE (YEARS)	HISTOPATHOLOGY	STAGE	CA125 (units/mL)		RESPONSE TO CHEMOTHERAPY COMBINATION OF CARBOPLATIN AND PACLITAXEL	PATIENT PHENOTYPE
				PRE-CHEMO	POST-CHEMO		
PA676	52	Papillary serous-adeno carcinoma	IIIC	980.5	7.1	Clinical and radiological disappearance of disease	Responder
RD304	53	Poorly differentiated endometroid-adeno carcinoma	IV	76.4	46.5	Developed multiple liver and umbilical metastasis at the end of 4 cycles	Non-responder
MD309	54	Serous cyst-adeno carcinoma	IIIC	>1000	74.5	Residual disease at the end of 6 cycles	Non-responder
SD482	70	Papillary serous cyst-adeno carcinoma	IIIC	166.9	2.0	Clinical and radiological disappearance of disease	Responder
US820	42	Papillary serous cyst-adeno carcinoma	IV	364.8	19.5	Clinical and radiological disappearance of disease	Responder
DD628	45	Papillary serous cyst-adeno carcinoma	IV	438.9	112	Clinical and radiological disappearance of disease	Non-responder
PK008	47	Clear cell carcinoma	IIIC	6230	4200	Presence of ascitic fluid	Non-responder
SM600	40	Serous cyst-adeno carcinoma	IIIC	1760	10.5	New lesion with lymph node at the end of 3 cycles	Non-responder
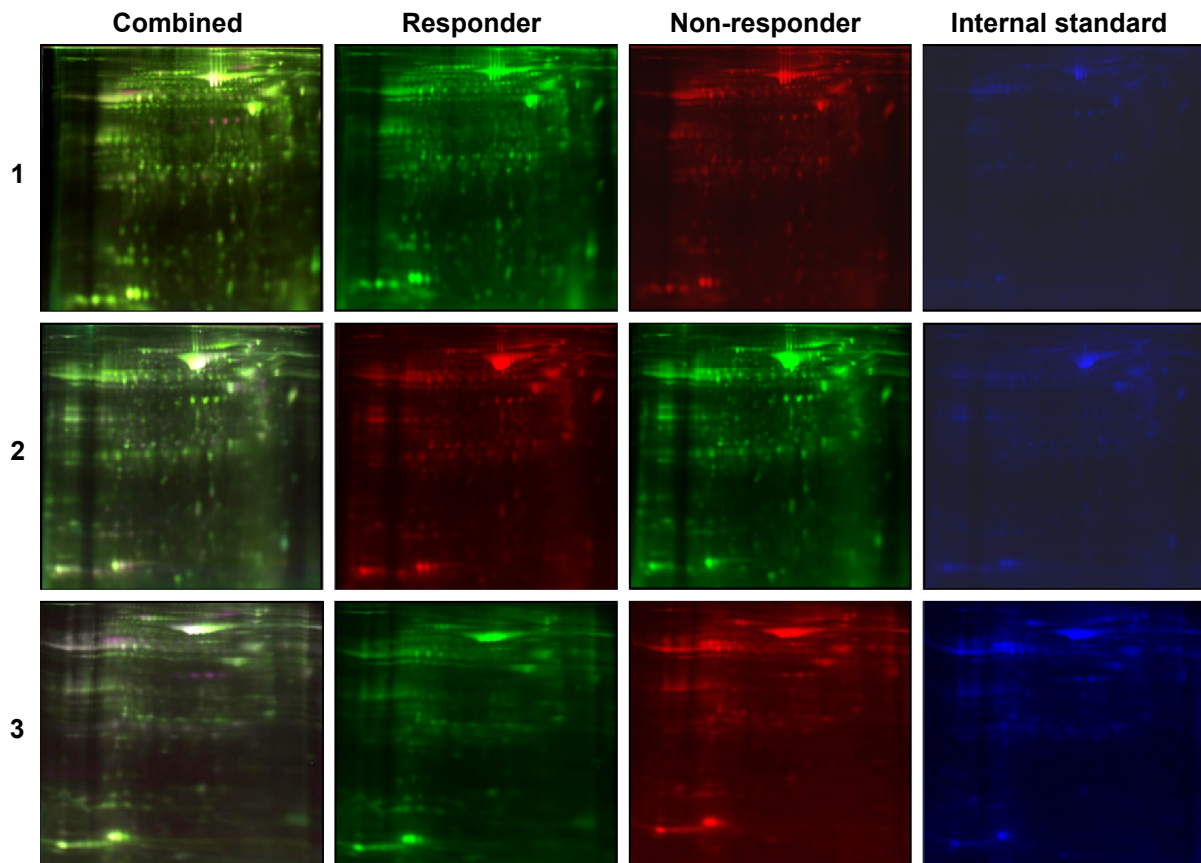
Figure 1. DIGE profile scans showing protein spots as a combined image, and individual images of responders, nonresponders, and internal standard. Responders and nonresponders were labeled with Cy3 and Cy5, respectively, in experiments 1 and 3, and labeled with Cy5 and Cy5, respectively, in experiment 2.

codetected in different DIA workspaces of *DeCyder* software. In biological variance analysis (BVA) module, Cy3 image from gel number one was chosen as master gel as it had the maximum number of spots. Eighteen spots were found to be differentially expressed with a criterion of: (1) being present in all nine images; (2) having average ratio more than +1.5 or less than −1.5, and (3) having a Student's *t*-test *P*-value <0.05. Spots are clearly visualized in the magnified gel images as shown in Figure 2. Analysis of the protein expression was done using *DeCyder* software, wherein the relative ratio of the spot was estimated based on the intensity, shown as volume of the peak covering the spot (Fig. 3). Relative ratio of expression was seen to be consistently maintained across all three sets of gels (Fig. 4). In the preparative gel stained with colloidal coomassie, nine spots were picked, trypsin digested and subjected to MS analysis, and identified with statistical significance. Average ratio of protein levels from the spots in the responders as compared with the nonresponders with the details from the *MASCOT* search results are given in Table 2. A snap shot of the *MASCOT* search results for all spots identified is provided as Supplementary Figure 1. Five proteins were upregulated and five proteins were downregulated in the responders as compared with the mean value of nonresponders.

**Proteins upregulated in nonresponders.**

A. Enoyl CoA hydratase is an important enzyme involved in beta-oxidation of polyunsaturated fatty acids.[31,32] Polyunsaturated fatty acids enhance cytotoxicity of several antineoplastic agents including cisplatin.[33,34] In another study, adding polyunsaturated fatty acids to the medium of cisplatin-resistant cells could enhance platinum sensitivity by increasing the binding capacity of platinum to DNA, with a consequent increase in the formation of platinum-DNA adducts.[35] Therefore, the sixfold overexpression of enoyl-CoA hydratase in the nonresponders is an indicator of a cell state deprived of polyunsaturated fatty acids making it vulnerable to platinum resistance. Enoyl-CoA hydratase knockdown also reduced cell viability and enhanced platinum induced apoptosis in cancer cells by Akt activation.[36] The identification of this protein provides evidence to the fact that mitochondrial defects cause ovarian cancer cell dysfunctions that were directly related to their resistance to platinum drugs.[37]

B. Prohibitin is present on mitochondrial inner membrane and has chaperonic functions. It is also involved in regulating proliferation and mitochondrial respiration regulation and aging. It was recently shown that overexpression
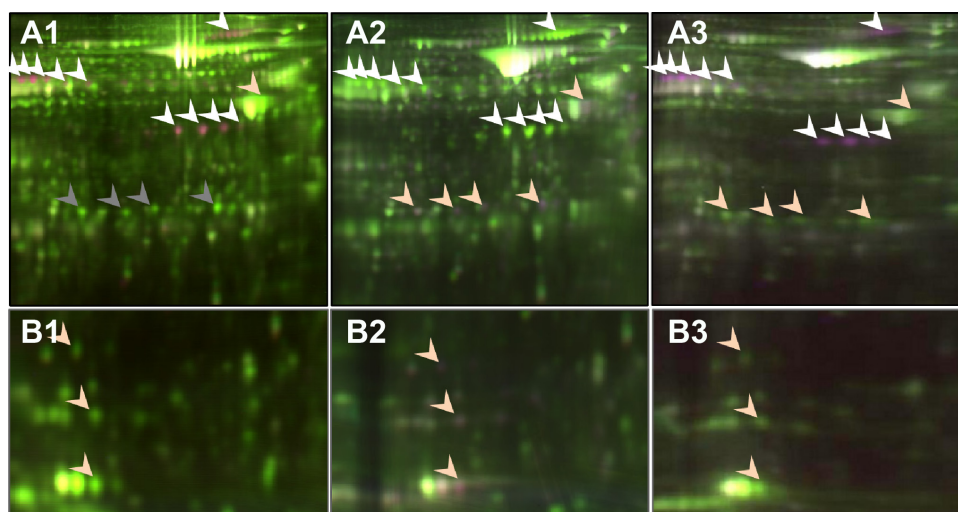
Figure 2. Magnified regions of combined gel image from three sets of experiments. **A1**, **A2**, and **A3** correspond to upper gel portion in the three gels. **B1**, **B2**, and **B3** correspond to lower gel portion in the three gels. Differentially expressed proteins assigned by DeCyder analysis are indicated by arrows. White arrows show overexpressed proteins in the ovarian cancer tissue of patient nonresponders and cream arrows show overexpressed proteins in the ovarian cancer tissue of patient responders.
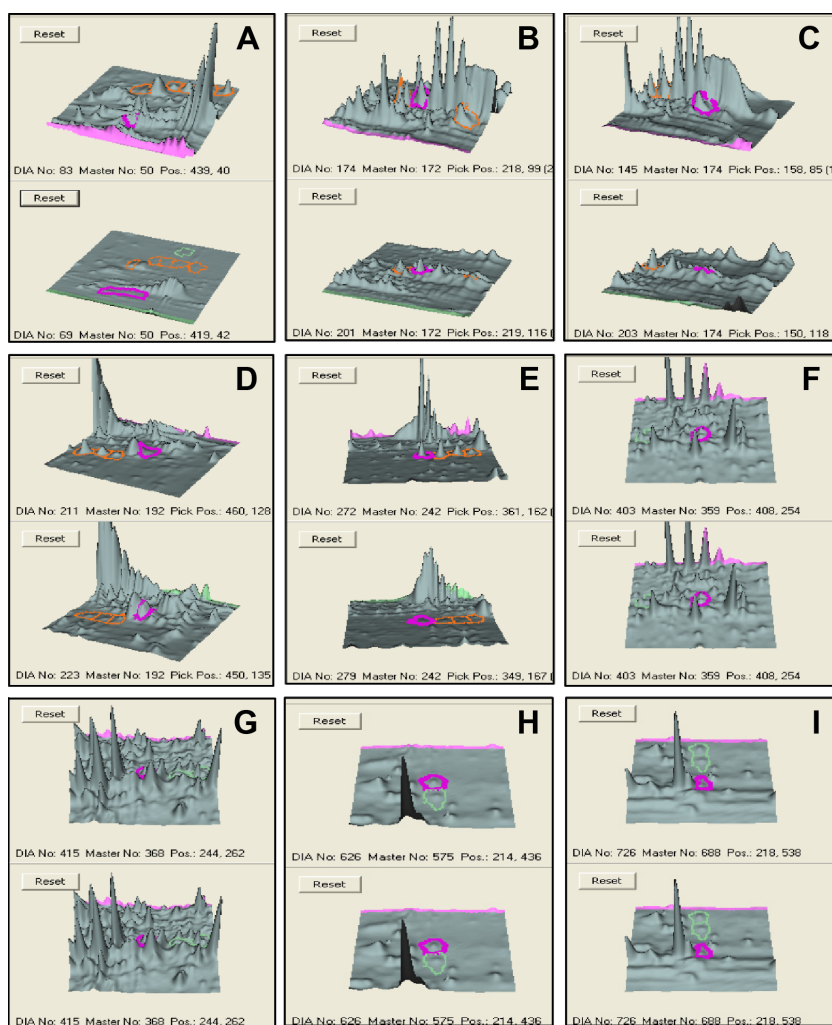
Figure 3. DeCyder software analysis. Spot intensities of corresponding peak volumes in the responder and nonresponder state of: (**A**) 50; (**B**) 172; (**C**) 174; (**D**) 192; (**E**) 242; (**F**) 359; (**G**) 368; (**H**) 575; and (**I**) 688.
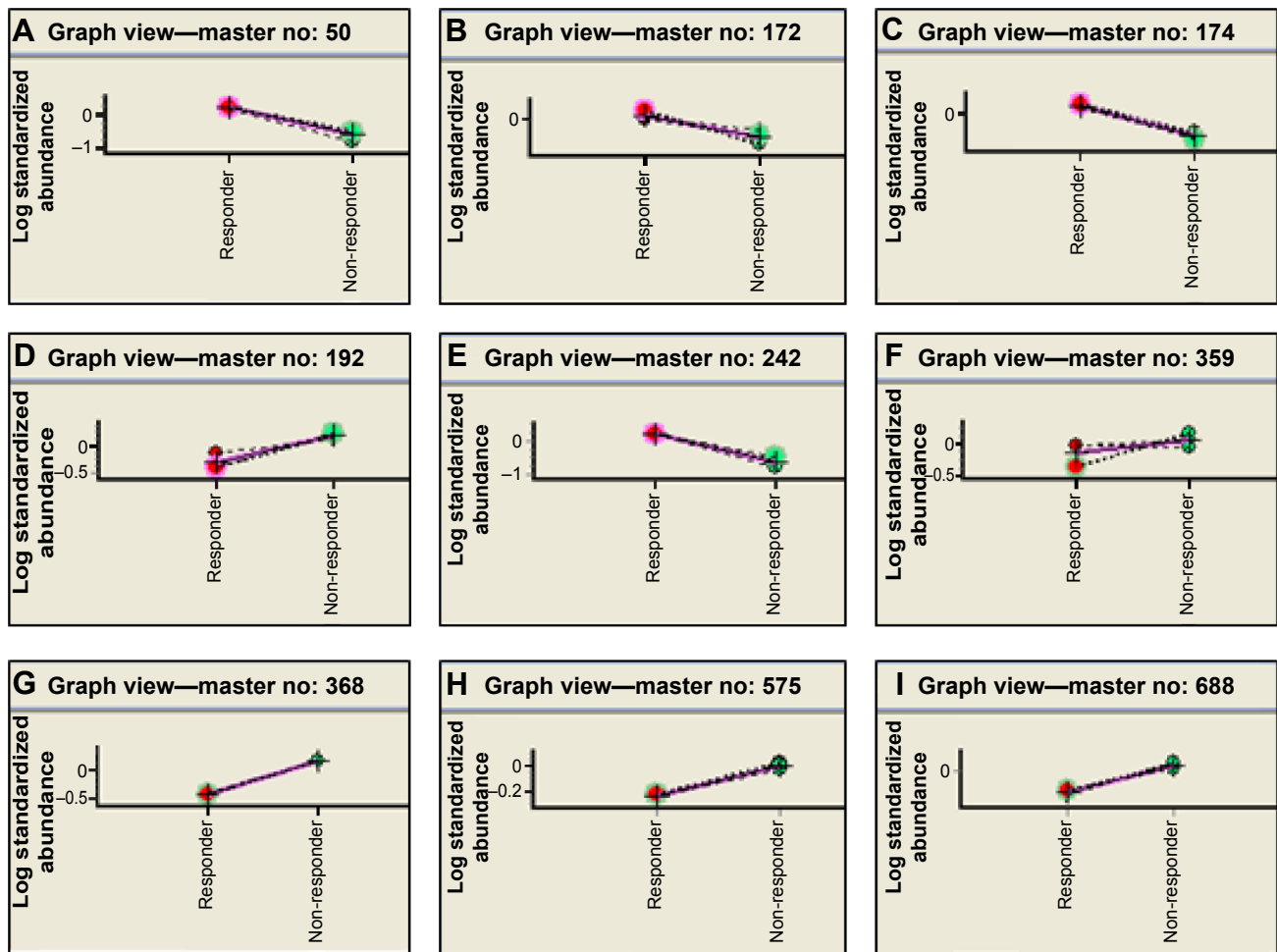
Figure 4. Relative abundance of differentially expressed proteins. Graphical representation of protein spots differentially expressed with volume ratio ±1.5 in cancer tissue from responders as compared with the nonresponders ($P < 0.05$). Data from the same gel are connected by dotted lines.

of prohibitin inhibits apoptosis, which concomitantly results in an increased level of the antiapoptotic proteins Bcl-2 and Bcl-xL, reduced release of cytochrome-C from mitochondria, and inhibition of caspase-3 activity.[38] Prohibitin inhibits apoptosis in ovarian cells through extracellular signal-regulated Mek-Erk1/2 and Bcl/Bcl-xL pathway. Prohibitin-mediated paclitaxel resistance is also mediated through Raf localization and Bcl-2 activation.[39] From the identified pool of differentially expressed proteins, prohibitin is one of the few proteins conferring paclitaxel resistance.

C. Peroxiredoxin-4 is involved in redox regulation of the cell. It also regulates the activation of NF-κB in the cytosol by a modulation of I-κB-alpha phosphorylation, thereby indirectly involved in the repression of reactive oxygen species (ROS)-mediated apoptosis.[40] Reducing peroxiredoxin 4 expression causes decreased cell growth and increased ROS. This leads to increased DNA damage and increased apoptosis.[41] Increased expression of peroxiredoxin 4 thus helps cancerous cells to overcome drug-induced stress by eliminating ROS and suppressing

programed cell death triggered by elevated levels of ROS apoptosis.

D. Fibrin β and fibrin γ are two proteins that are upregulated in the nonresponder tissue with more than five-fold difference. From a functional perspective, their role in chemotherapy resistance is multifold and they (a) have cumulative effects in increasing angiogenesis thus increases nutrient supply to the cancerous cell to promote their growth;[42] (b) improve cell survival and reduces apoptosis by increasing resistance to ROS;[43] (c) reflect decreased fibrin degradation products which in turn decrease caveolin-1-mediated apoptosis;[44] and (d) provide matrix support to the cancer cells, augmenting their growth.[45]

E. α-Enolase is a metabolic enzyme and is called as *platinum drug chemo-resistant factor* and is upregulated in platinum-resistant cells.[46,47] The proposed theories for chemotherapy resistance are (a) α-enolase loses its glycolytic activity, which is very essential for the antitumor action of cisplatin;[48] (b) α-enolase–tubulin interactions modulates microtubule network, thereby causing resistance to

Table 2. List of differentially expressed proteins.

NO.	SPOT	IDENTIFIED PROTEIN	UNIPROT ID	ACCESSION NO.	EXPERIMENTAL MASS (kDa)/pI	THEORETICAL MASS (kDa)/pI	AVERAGE RATIO (R:NR)	APPEARANCE IN GEL	MASCOT SCORE	NO. OF PEPTIDES IDENTIFIED	COVERAGE (%)
1	50	Fibrin γ	P02679	gi|182439	87.09/5.2	49.45/5.6	−5.6	9(9)	152	4	13
2	172	α-enolase 1	P06733	gi|4503571	50.11/7.8	47.1/7.0	−1.5	9(9)	91	4	12
3	174	Fibrin β	P02675	gi|223002	52.48/8.4	50.7/7.9	−7.8	9(9)	576	11	27
4	192	Actin 1	P60709	gi|4501885	41.68/4.9	41.7/5.29	+2.9	9(9)	277	6	28
5	242	Enoyl coA hydratase	P30084	gi|433413	39.81/6.1	31.2/8.0	−6.2	9(9)	49	1	7
6	242	Peroxiredoxin 4	Q13162	gi|5453549	39.81/6.2	30.5/5.8	−6.2	9(9)	39	1	5
7	242	Prohibitin 1	P35232	gi|4505773	39.81/6.3	29.7/5.5	−6.2	9(9)	233	6	33
8	359	hnRNP	P31942	gi|7739445	28.84/5.7	31.5/6.7	+1.6	9(9)	90	1	5
9	359	Aldose reductase	P15121	gi|225939	28.84/5.8	36.3/6.3	+1.6	9(9)	108	2	8
10	368	Heat shock protein 27	P04792	gi|662841	28.84/7.5	22.3/7.83	+3.9	9(9)	94	3	17
11	575	Cyclophilin A	P62937	gi|1633054	17.37/8.3	17.8/7.8	+1.8	9(9)	142	5	35
12	688	β-globin	Q4TWB7	gi|179409	8.96/8.1	15.8/7.8	+4.4	9(9)	291	5	35

microtubule-targeted drugs such as paclitaxel;[49] (c) in the cell membrane of apoptotic cells, α-enolase acts as plasminogen receptor promoting cellular metabolism in anaerobic conditions and driving tumor invasion through plasminogen activation and extracellular matrix degradation, activating intracellular survival pathway and controlling cell apoptosis;[50,51] and (d) α-enolase also inhibits apoptosis partly.[40] Overexpression of this protein in the tissue of patients not responding to carboplatin further validates and reiterates these studies.

Proteins upregulated in responders.

A. HSP-27 is a cytosolic chaperonic protein that is expressed as a stress response. It assists in the formation or maintenance of the native conformation of cytosolic proteins and actin organization. The coexpression of these two proteins, HSP-27 and actin, is very relevant in understanding ovarian cancer cell sensitivity to chemotherapy. HSP-27 interacts with p66shc and accelerates cisplatin-dependent disruption of the actin cytoskeleton and consequently cancer cell apoptosis, a mechanism that confers drug sensitivity.[52] In addition, HSP-27 regulates the ABC transporters MDR1 and P-gp-based efflux transporters, causing drug to be retained in the cancerous cells for a longer time, and induced apoptosis by increasing G(2)/M population.[53]

B. Actin, independently, has functional roles in making cells chemotherapy sensitive. It (a) initiates the intrinsic pathway of apoptosis as microfilament assembly is a necessary factor for formation of apoptotic bodies in later stages of apoptosis.[54] and (b) is involved in Bcl2-mediated cell death.[55]

C. hnRNP is a nuclear protein that functions in mRNA processing. There are several functional consequences of alternating splicing on apoptosis.[56] A delicate balance between the activities of pro- and antiapoptotic variants produced by APAF-1, Bcl-xL, Fas, and caspases is often controlled through alternative splicing, and a number of studies have documented the contribution of hnRNP and hnRNP-like proteins in the control of splice site selection in apoptotic genes.[57] Therefore, overexpression of hnRNP in responder state helps to trigger effective alternating splicing of apoptotic genes leading to enhancement of apoptotic event upon chemotherapeutic stress.

D. Aldose reductase is a nicotinamide adenine dinucleotide phosphate dehydrogenase (NADPH)-dependent aldo-keto reductase enzyme. Overexpression of aldose reductase induces apoptosis by triggering DNA fragmentation, regulating TNF-α signaling and suppression of NF-kb activity.[58,59] Therefore, it may influence the sensitivity of cells to chemotherapy.

Differentially expressed proteins, apoptosis, and chemotherapy response. In order to decipher the relevant role of
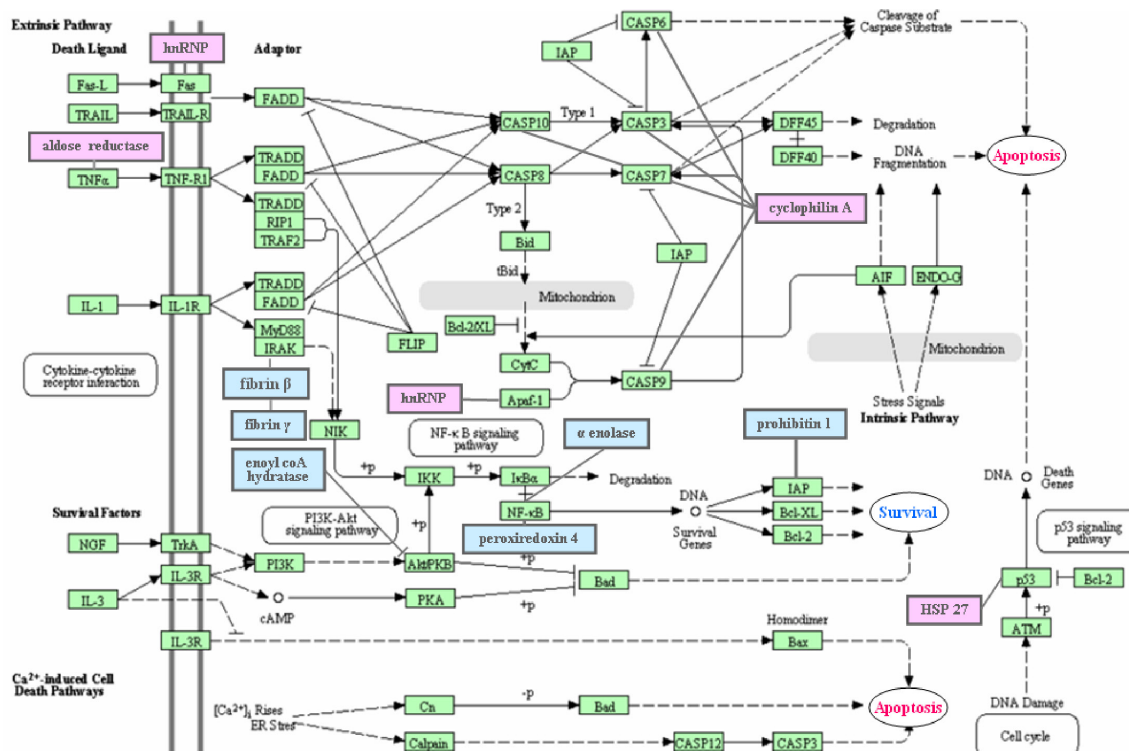
Table 3. List of differentially expressed proteins, interacting partners, and activated pathways.

PROTEIN	INTERACTING PROTEINS	PATHWAY	REFERENCE
Aldose reductase	TNF-α	Apoptosis	58,59
hnRNP	Collapsin response mediator protein 1 Apaf-1	Apoptosis	57,60
HSP-27	p53	Apoptosis	60
Cyclophilin A	Caspases 3, Caspase 6, Caspase 7, Caspase 9	Apoptosis	61
Prohibitin	Raf-1 Proto-Oncogene Histone Deacetylase 1 E2F transcription factor 1 Retinoblastoma 1	Survival	62–65
β-actin	Chaperonin containing TCP1, Subunit 5 LIM and SH3 Protein 1	Survival	66,67
α-enolase	NF-κb	Survival	68
β and γ fibrin	IRAK	Survival	69,70
Enoyl coA hydratase	Akt pκb	Survival	36
Prohibitin 1	Bcl-2	Survival	39
Peroxiredoxin 4	NF-κb	Survival	40

these proteins with respect to response in two clinical states, it becomes imperative to understand the biology of ovarian carcinogenesis and chemotherapy effect, which is mediated by inducing apoptosis in cancer cells. Therefore, a pathway analysis was carried out to look at the possible interactions mediated by the differentially expressed proteins in regulating apoptosis and cancer. A total of 371 genes were mapped in cancer regulation, 105 genes were mapped in apoptosis regulation, and 45 genes were common between the two regulatory networks. The interactions are summarized in Table 3. A brief overview of apoptotic and survival pathways are illustrated vis-à-vis the functional interactions of the identified proteins in Figure 5.

Figure 5. KEGG pathway analysis.[71,72] The integrated pathway showing the interactions of differentially expressed proteins in apoptotic and survival pathways. Apoptotic and survival pathway proteins are boxed in green color. The over expressed proteins in responders are boxed in pink color and the overexpressed proteins in nonresponders are boxed in light blue color. Bold lines indicate interaction, dotted lines indicate reaction series, and lines ending with vertical bars indicate inhibition.

**Table 4.** Details of primer used for RT-PCR quantification.

GENE	FORWARD PRIMER (5′-3′)	REVERSE PRIMER (5′-3′)
α-enolase	ACTGAAGATACCTTCATCGCTG	CTCTTCAATTCTGAGGAGCTG
HSP-27	CTACATCTCCCGGTGCTTCA	TCTCGTTGGACTGCGTGGCT
Caspase 3	CAGAACTGG ACTGTGGCATTG	AACCAGGTGCTGTGGAGTATG
Caspase 8	ACCACGACCTTTGAAGAGCTT	ATGTTACTGTGGTCCATGAGT
Cytochrome C	CAAATCTCCATGGTCTCTTTG	TCTCCAAATACTCCATCAGTG
GAPDH	ATCCTGGGCTACACTGAGCA	ATGAGCTTGACAAAGTGGTCG

Apoptosis is a highly regulated biological process comprising of programed array of molecular events, which helps the body to get rid of unwanted cells. Apoptosis is mediated by two independent pathways: (a) extrinsic or death receptor-mediated pathway and (b) intrinsic or mitochondrial pathway. Among the upregulated proteins in responders, aldose reductase interacts with the ligands TRAIL and TNF-α; hnRNP interacts with Fas-receptor through CRMP1, and cyclophilin A interacts with an array of effector caspases. The intrinsic pathway of apoptosis is initiated within the cell by certain stimuli and involves a wide array of intracellular signaling events that increase mitochondrial permeability and release proapoptotic molecules such as cytochrome C and AIF into the cytoplasm. Cytochrome C along with Apaf-1 and caspase 9 form a complex, apoptosome, which activates caspase 3. This pathway is inhibited by Bcl-2, Bcl-xL, Bcl-W, Bfl-1, and Mcl-1 and activated by Bak, Bax, Bad, Bcl-xS, Bid, Bim, and Hrk. Among the proteins identified, hnRNP interacts with Apaf-1 and cyclophilin A interacts with caspases 9. Intrinsic and extrinsic pathways converge on caspase 3 that effects nuclear fragmentation, cytoskeletal reorganization, and disintegration of the cell into apoptotic bodies. In addition, activation of Ras and AKT pathways inactivates the proapoptotic molecules and p53 initiates apoptosis. Also simultaneously, TNF-α and IL1, through NF-κB signaling pathway, and NGF and IL3, through Akt signaling pathway, mediate cell survival. While fibrin-γ and fibrin-β are seen to have interactions with IRAK, most of the other nonresponder proteins including α-enolase, prohibitin,

enoyl-coA hydratase, and peroxiredoxin show interactions with molecules in the NF-κB cell survival pathway, which is clinically a chemotherapy-resistant state.

This helps to understand that cells are in an innately dictated preconditioned balance between apoptotic and cancer cell cycles. The alterations in these pathways play a vital role in determining chemotherapy response. The interactions made by the identified proteins with proteins in cancer, apoptosis, and common gene pool provide a conceptual framework that explains innately driven mechanisms of resistance and sensitivity to chemotherapy.

Expression and functional validation. Based on the pathway analysis, interaction network, and functional relevance, HSP-27 and α-enolase were chosen for tissue transcript analysis for validation. The sequences of the primers used are shown in Table 4. Between responders and nonresponders, the fold change mRNA expression of HSP-27 was +2.3 that for α-enolase was −1.4 (Fig. 6A). These results are comparable with the relative expression ratios between the responders and nonresponders for the same proteins. Caspases 8, caspase 3, and cytochrome C were considered as markers for intrinsic, extrinsic, and final common pathways in apoptosis, respectively. It is seen that expressions of these genes are relatively more in the responders as compared with the nonresponders (Fig. 6B). This suggests of an increased apoptotic activity in the responders and, therefore, explains their sensitivity to chemotherapy. Furthermore, correlation studies of biomarker proteins HSP-27 and α-enolase with the three apoptotic proteins show a moderate amount of association
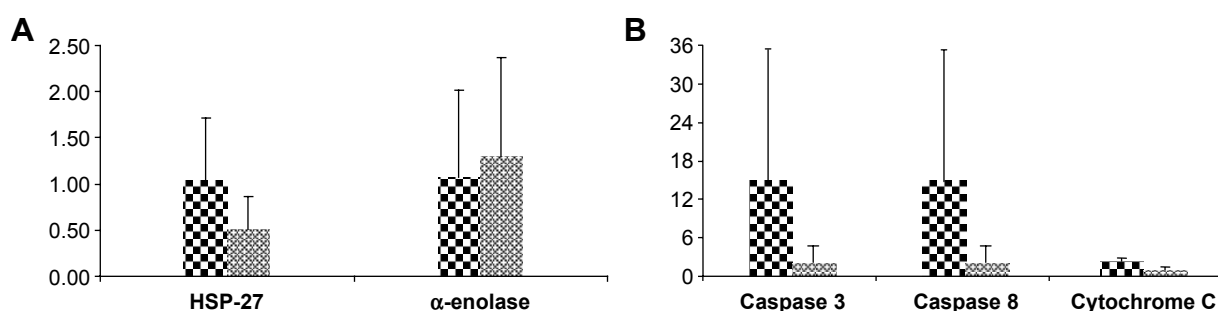
Figure 6. Relative mRNA expression of (**A**) differentially expressed proteins: HSP-27, and α-enolase; (**B**) apoptotic proteins: caspases 3, caspases 8, and cytochrome C. Mean and standard deviation are plotted in histogram with plus one standard deviation. Bar diagrams for responders are shown in thick checkered boxes and bar diagrams for nonresponders are shown in thin checkered boxes.
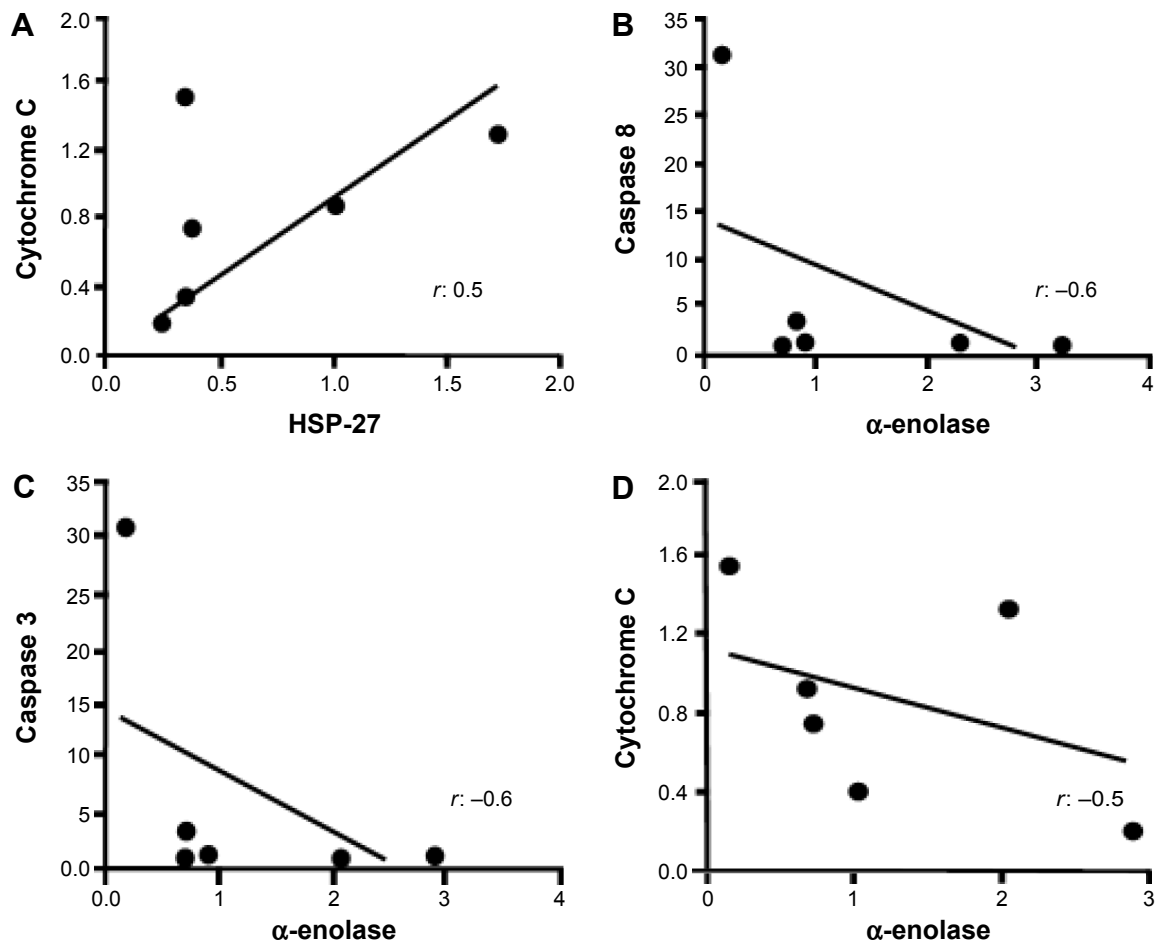
Figure 7. Correlation analysis for mRNA expression between (**A**) HSP-27 and cytochrome C; (**B**) α-enolase and caspase 8; (**C**) α-enolase and caspase 3; and (**D**) α-enolase and cytochrome C.

with correlation coefficient (*r*) values of ±0.5 (Fig. 7). A couple of outliers have resulted in skewing the strength of correlation. A larger cohort would help to strengthen the correlation. At the proteome level, Western blot experiments confirm the differential expression of α-enolase between the responders and nonresponders (Fig. 8). Though the study is done on a small sample size, the trend shown by these validation experiments augurs well for analysis on a larger cohort of tissue and serum samples.

Conclusion

There are differentially expressed proteins that bestow innate drug-sensitive and -resistant states to advanced ovarian cancer patients receiving combination chemotherapy of paclitaxel and carboplatin. While aldehyde reductase, hnRNP, cyclophilin A, HSP-27, and actin are upregulated in the responder state, prohibitin, enoyl-coA hydratase, peroxiredoxin, and fibrin-β are upregulated in the nonresponder state. The inherent proteins, HSP-27, and α-enolase, either individually or as a panel, are potential biomarkers that can predict carboplatin–paclitaxel treatment response. These proteins are intricately related to cell apoptotic pathways and are thereby
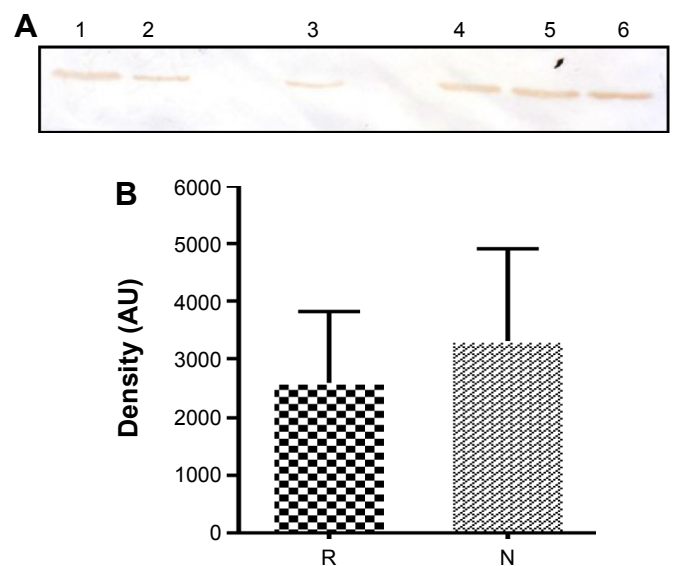
Figure 8. Western blot analysis of α-enolase. (**A**) Bands corresponding to α-enolase in ovarian cancer tissue of responders (1–2) and nonresponders (3–6). (**B**) Mean and standard deviation of band densities are plotted in histogram with plus one standard deviation. Bar diagrams for responders and nonresponders are shown in thick checkered thin checkered boxes, respectively.

functionally and clinically relevant. This study is an ideal platform for designing diagnostics and drug target identification, to assist clinicians and patients in the chemotherapeutics of advanced ovarian cancer.

Acknowledgments

Author Contributions

Conceived and designed the experiments: GH. Carried out the experiments: US, RP, AKG, RH, MIK, DG, JN, and PV. Analyzed the data: GH, LK, and SK. Wrote the first draft of the manuscript: GH. Contributed to the writing of the manuscript: GH, LK, and SK. Agreed with manuscript results and conclusions: GH, LK, SK, AKM, SBS, and PV. Jointly developed the structure and arguments for the paper: GH, LK, SK, AKM, SBS, and PV. Made critical revisions and approved the final version: GH, US, RP, AKG, RH, MIK, DG, JN, LK, SK, PV, AKM, and SBS. All the authors reviewed and approved the final manuscript.

Supplementary Material

Supplementary figure 1. Snap shot of protein identification using MASCOT software.

REFERENCES

1. Ferlay J, Soerjomataram I, Ervik M, et al. *GLOBOCAN 2012 v1.0, Cancer Incidence and Mortality Worldwide*. Lyon, France: IARC CancerBase No. 11; 2012. [Internet].
2. International Agency for Research on Cancer. *GLOBOCAN 2012: Estimated Cancer Incidence, Mortality and Prevalence Worldwide in 2012*. Lyon, France: International Agency for Research on Cancer; World Health Organization; 2012. Available at: http://globocan.iarc.fr/Pages/fact_sheets_cancer.aspx. Section on Cancer Information.
3. Chen LM, Berek JS. Ovarian and fallopian tubes. In: Haskell CM, ed. *Cancer Treatment*. 5th ed. Philadelphia, PA: WB Saunders; 2000:55.
4. Hainsworth JD, Thompson DS, Bismayer JA, et al. Paclitaxel/carboplatin with or without sorafenib in the first-line treatment of patients with stage III/IV epithelial ovarian cancer: a randomized phase II study of the Sarah Cannon Research Institute. *Cancer Med*. 2015;4(5):673–681. doi: 10.1002/cam4.376.
5. Raymond E, Faivre S, Woynarowski JM, Chaney SG. Oxaliplatin: mechanism of action and antineoplastic activity. *Semin Oncol*. 1998;25(2 suppl 5):4–12.
6. Parness J, Horwitz SB. Taxol binds to polymerized tubulin in vitro. *J Cell Biol*. 1981;91(1):479–487.
7. Manfredi JJ, Parness J, Horwitz SB. Taxol binds to cellular microtubules. *J Cell Biol*. 1982;94(3):688–696.
8. du Bois A, Lück HJ, Meier W, et al. Arbeitsgemeinschaft Gynäkologische Onkologie Ovarian Cancer Study Group. *J Natl Cancer Inst*. 2003;95(17):1320–1329.
9. International Collaborative Ovarian Neoplasm Group. Paclitaxel plus carboplatin versus standard chemotherapy with either single-agent carboplatin or cyclophosphamide, doxorubicin, and cisplatin in women with ovarian cancer: the ICON3 randomized trial. *Lancet*. 2002;360(9332):505–515.
10. Markman M, Rothman R, Hakes T, et al. Second-line platinum therapy in patients with ovarian cancer previously treated with cisplatin. *J Clin Oncol*. 1991;9(3):389–393.
11. Gore ME, Fryatt I, Wiltshaw E, Dawson T. Treatment of relapsed carcinoma of the ovary with cisplatin or carboplatin following initial treatment with these compounds. *Gynecol Oncol*. 1990;36(2):207–211.
12. Meads MB, Gatenby RA, Dalton WS. Environment-mediated drug resistance: a major contributor to minimal residual disease. *Nat Rev Cancer*. 2009;9(9):665–674.
13. Khaider NG, Lane D, Matte I, Rancourt C, Piché A. Targeted ovarian cancer treatment: the TRAILs of resistance. *Am J Cancer Res*. 2012;2(1):75–92.
14. Xu M, Takanashi M, Oikawa K, et al. Identification of a novel role of Septin 10 in paclitaxel-resistance in cancers through a functional genomics screen. *Cancer Sci*. 2012;103(4):821–827.
15. Di Michele M, Marcone S, Cicchillitti L, et al. Glycoproteomics of paclitaxel resistance in human epithelial ovarian cancer cell lines: towards the identification of putative biomarkers. *J Proteomics*. 2010;73(5):879–898.
16. Hariprasad G, Hariprasad R, Kumar L, Srinivasan A, Kola S, Kaushik A. Apolipoprotein A1 as a potential biomarker in the ascitic fluid for the differentiation of advanced ovarian cancers. *Biomarkers*. 2013;18(6):532–541.
17. Kataria J, Rukmangadachar AL, Hariprasad G, Tripathi M, Srinivasan A. Cerebrospinal fluid proteomics in tuberculus meningitis patients. *J Proteomics*. 2011;74(10):2194–2203.
18. Rukmangadachar LA, Kataria J, Hariprasad G, Samantaray JC, Srinivasan A. Two-dimensional difference gel electrophoresis (DIGE) analysis of sera from visceral leishmaniasis patients. *Clin Proteomics*. 2011;8(1):4.
19. Della Pepa C, Tonini G, Pisano C, et al. Ovarian cancer standard of care: are there real alternatives? *Chin J Cancer*. 2015;34(1):17–27.
20. Walters Haygood CL, Arend RC, Straughn JM, Buchsbaum DJ. Ovarian cancer stem cells: can targeted therapy lead to improved progression-free survival? *World J Stem Cells*. 2014;6(4):441–447.
21. Drerup JM, Liu Y, Padron AS, et al. Immunotherapy for ovarian cancer. *Curr Treat Options Oncol*. 2015;16(1):317.
22. Hariprasad G, Srinivasan A, Vedakumari Y. Electrical conductivity as a tool to detect salt in clinical proteomics samples. *Indian J Clin Biochem*. 2011;26:82–83.
23. Pokhriyal R, Basnet B, Gupta AK, Sehrawat U, Jain SK, Hariprasad G. Effect of lipid on gel based electrophoretic proteomic experiments. *J Proteins Proteomics*. 2014;5(2):121–124.
24. Kanehisa M. The KEGG database. *Novartis Found Symp*. 2002;247:91–101.
25. Smoot M, Ono K, Ruscheinski J, Wang P, Ideker T. Cytoscape 2.8: new features for data integration and network visualization. *Bioinformatics*. 2011;27(3):431–432.
26. Shannon P, Markiel A, Ozier O, et al. Cytoscape: a software environment for integrated models of biomolecular interaction networks. *Genome Res*. 2003;13(11):2498–2504.
27. Gao J, Ade AS, Tarcea VG, et al. Integrating and annotating the interactome using the MiMI plugin for cytoscape. *Bioinformatics*. 2009;25(1):137–138.
28. Bader GD, Betel D, Hogue CWV. BIND: the biomolecular interaction network database. *Nucleic Acids Res*. 2003;31:248–250.
29. Chatr-aryamontri A, Ceol A, Palazzi LM, et al. MINT: the molecular interaction database. *Nucleic Acids Res*. 2007;35(suppl 1):D572–D574.
30. Prasad KTS, Goel R, Kandasamy K, et al. Human protein reference database—2009 update. *Nucleic Acids Res*. 2009;37(Database issue):D767–D772.
31. Uchida Y, Izai K, Orii T, Hashimoto T. Novel fatty acid beta-oxidation enzymes in rat liver mitochondria. II. Purification and properties of enoyl-coenzyme A (CoA) hydratase/3-hydroxyacyl-CoA dehydrogenase/3-ketoacyl-CoA thiolase trifunctional protein. *J Biol Chem*. 1992;267(2):1034–1041.
32. Kamijo T, Wanders RJ, Saudubray JM, Aoyama T, Komiyama A, Hashimoto T. Mitochondrial trifunctional protein deficiency. Catalytic heterogeneity of the mutant enzyme in two patients. *J Clin Invest*. 1994;93(4):1740–1747.
33. Conklin KA. Dietary polyunsaturated fatty acids: impact on cancer hemotherapy and radiation. *Altern Med Rev*. 2002;7(1):4–21.
34. Warmoes M, Jaspers JE, Xu G, et al. Proteomics of genetically engineered mouse mammary tumors identifies fatty acid metabolism members as potential predictive markers for cisplatin resistance. *Mol Cell Proteomics*. 2013;12(5):1319–1334.
35. Timmer-Bosscha H, Hospers GA, Meijer C, et al. Influence of docosahexaenoic acid on cisplatin resistance in a human small cell lung carcinoma cell line. *J Natl Cancer Inst*. 1989;81(14):1069–1075.
36. Zhu XS, Dai YC, Chen ZX, et al. Knockdown of ECHS1 protein expression inhibits hepatocellular carcinoma cell proliferation via suppression of Akt activity. *Crit Rev Eukaryot Gene Expr*. 2013;23(3):275–282.
37. Dai Z, Yin J, He H, et al. Mitochondrial comparative proteomics of human ovarian cancer cells and their platinum-resistant sublines. *Proteomics*. 2010;10(21):3789–3799.
38. Chowdhury I, Thompson WE, Welch C, Thomas K, Matthews R. Prohibitin (PHB) inhibits apoptosis in rat granulosa cells (GCs) through the extracellular signal-regulated kinase 1/2 (ERK1/2) and the Bcl family of proteins. *Apoptosis*. 2013;18(12):1513–1525.
39. Patel N, Chatterjee SK, Vrbanac V, et al. Rescue of paclitaxel sensitivity by repression of prohibitin1 in drug-resistant cancer cells. *Proc Natl Acad Sci U S A*. 2010;107(6):2503–2508.
40. Yang S, Luo A, Hao X, et al. Peroxiredoxin 2 inhibits granulosa cell apoptosis during follicle atresia through the NFKB pathway in mice. *Biol Reprod*. 2011;84(6):1182–1189.
41. Kim TH, Song J, Alcantara Llaguno SR, et al. Suppression of peroxiredoxin 4 in glioblastoma cells increases apoptosis and reduces tumor growth. *PLoS One*. 2012;7(8):e42818.
42. Hinsbergh VW, Collen A, Koolwijk P. Role of fibrin matrix in angiogenesis. *Ann N Y Acad Sci*. 2001;936:426–437.

43. Kuehn C, Lakey JR, Lamb MW, Vermette P. Young porcine endocrine pancreatic islets cultured in fibrin show improved resistance toward hydrogen peroxide. *Islets*. 2013;5(5):207–215.

44. Guo YH, Hernandez I, Isermann B, et al. Caveolin-1-dependent apoptosis induced by fibrin degradation products. *Blood*. 2009;113(18):4431–4439.

45. Shikanov A, Xu M, Woodruff TK, Shea LD. Interpenetrating fibrin-alginate matrices for in vitro ovarian follicle development. *Biomaterials*. 2009;30(29): 5476–5485.

46. Nishimura K, Tsuchiya Y, Okamoto H, et al. Identification of chemoresistant factors by protein expression analysis with iTRAQ for head and neck carcinoma. *Br J Cancer*. 2014;111(4):799–806.

47. Kageyama T, Nagashio R, Ryuge S, et al. HADHA is a potential predictor of response to platinum-based chemotherapy for lung cancer. *Asian Pac J Cancer Prev*. 2011;12(12):3457–3463.

48. Li Z, Zhao X, Yang J, Wei Y. Proteomics profile changes in cisplatin-treated human ovarian cancer cell strain. *Sci China C Life Sci*. 2005;48(6):648–657.

49. Georges E, Bonneau AM, Prinos P. RNAi-mediated knockdown of alpha-enolase increases the sensitivity of tumor cells to antitubulin chemotherapeutics. *Int J Biochem Mol Biol*. 2011;2(4):303–308.

50. Díaz-Ramos A, Roig-Borrellas A, García-Melero A, López-Alemany R. α-enolase, a multifunctional protein: its role on pathophysiological situations. *J Biomed Biotechnol*. 2012;2012:156795.

51. Capello M, Ferri-Borgogno S, Cappello P, Novelli F. α-Enolase: a promising therapeutic and diagnostic tumor target. *FEBS J*. 2011;278(7):1064–1074.

52. Arany I, Clark JS, Reed DK, Ember I, Juncos LA. Cisplatin enhances interaction between p66Shc and HSP27: its role in reorganization of the actin cytoskeleton in renal proximal tubule cells. *Anticancer Res*. 2012;32(11):4759–4763.

53. Kanagasabai R, Krishnamurthy K, Druhan LJ, Ilangovan G. Forced expression of heat shock protein 27 (Hsp27) reverses P-glycoprotein (ABCB1)-mediated drug efflux and MDR1 gene expression in adriamycin-resistant human breast cancer cells. *J Biol Chem*. 2011;286(38):33289–33300.

54. Cotter TG, Lennon SV, Glynn JM, Green DR. Microfilament-disrupting agents prevent the formation of apoptotic bodies in tumor cells undergoing apoptosis. *Cancer Res*. 1992;52(4):997–1005.

55. Martin SS, Leder P. Human MCF10A mammary epithelial cells undergo apoptosis following actin depolymerization that is independent of attachment and rescued by Bcl-2. *Mol Cell Biol*. 2001;21(19):6529–6536.

56. Schwerk C, Schulze-Osthoff K. Regulation of apoptosis by alternative pre-mRNA splicing. *Mol Cell*. 2005;19(1):1–13.

57. Garneau D, Revil T, Fisette JF, Chabot B. Heterogeneous nuclear ribonucleoprotein F/H proteins modulate the alternative splicing of the apoptotic mediator Bcl-x. *J Biol Chem*. 2005;280(24):22641–22650.

58. Hamaoka R, Fujii J, Miyagawa J, et al. Overexpression of the aldose reductase gene induces apoptosis in pancreatic beta-cells by causing a redox imbalance. *J Biochem*. 1999;126(1):41–47.

59. Ramana KV, Bhatnagar A, Srivastava SK. Aldose reductase regulates TNF-alpha-induced cell signaling and apoptosis in vascular endothelial cells. *FEBS Lett*. 2004;570(1–3):189–194.

60. Stelzl U, Worm U, Lalowski M, et al. A human protein-protein interaction network: a resource for annotating the proteome. *Cell*. 2005;122(6):957–968.

61. Capno M, Virji S, Crompton M. Cyclophilin-A is involved in excitotoxin-induced caspase activation in rat neuronal B50 cells. *Biochem J*. 2002;363(1):29–36.

62. Chiu CF, Ho MY, Peng JM, et al. Raf activation by *Ras* and promotion of cellular metastasis require phosphorylation of prohibitin in the raft domain of the plasma membrane. *Oncogene*. 2013;32(6):777–787.

63. Toska E, Shandilya J, Goodfellow SJ, Medler KF, Roberts SG. Prohibitin is required for transcriptional repression by the WT1-BASP1 complex. *Oncogene*. 2014;33(43):5100–5108.

64. Wang S, Zhang B, Faller DV. Prohibitin requires Brg-1 and Brm for the repression of E2F and cell growth. *EMBO J*. 2002;21(12):3019–3028.

65. Wang S, Nath N, Adlam M, Chellappan S. Prohibitin, a potential tumor suppressor, interacts with RB and regulates E2F function. *Oncogene*. 1999;18(23): 3501–3510.

66. McCormack EA, Llorca O, Carrascosa JL, Valpuesta JM, Willison KR. Point mutations in a hinge linking the small and large domains of beta-actin result in trapped folding intermediates bound to cytosolic chaperonin CCT. *J Struct Biol*. 2001;135(2):198–204.

67. Orth MF, Cazes A, Butt E, Grunewald TG. An update on the LIM and SH3 domain protein 1 (LASP1): a versatile structural, signaling, and biomarker protein. *Oncotarget*. 2015;6(1):26–42.

68. Choi J, Kim H, Kim Y, et al. The anti-inflammatory effect of GV1001 mediated by the downregulation of ENO1-induced pro-inflammatory cytokine production. *Immune Netw*. 2015;15(6):291–303.

69. Kuhns DB, Priel DA, Gallin JI. Induction of human monocyte interleukin (IL)-8 by fibrinogen through the toll-like receptor pathway. *Inflammation*. 2007;30(5): 178–188.

70. Li YW, Mo XB, Zhou L, et al. Identification of IRAK-4 in grouper (*Epinephelus coioides*) that impairs MyD88-dependent NF-κB activation. *Dev Comp Immunol*. 2014;45(1):190–197.

71. Kanehisa M, Sato Y, Kawashima M, Furumichi M, Tanabe M. KEGG as a reference resource for gene and protein annotation. *Nucleic Acids Res*. 2016;44: D457–D462.

72. Kanehisa M, Goto S. KEGG: Kyoto Encyclopedia of Genes and Genomes. *Nucleic Acids Res*. 2000;28:27–30.